ASM Handbook, Volume 10: Materials Characterizations
R.E. Whan, editor, p 610-627
DOI: 10.31399/asm.hb.v10.a0001774

Secondary Ion Mass Spectroscopy

Carlo G. Pantano, Department of Materials Science and Engineering, The Pennsylvania State University

General Uses

- Surface compositional analysis with approximately 5- to 10-nm depth resolution
- Elemental in-depth concentration profiling
- Trace element analysis at the parts per billion to parts per million range
- Isotope abundances
- Hydrogen analysis
- Spatial distribution of elemental species

Examples of Applications

- Identification of inorganic or organic surface layers on metals, glasses, ceramics, thin films, or powders
- In-depth composition profiles of oxide surface layers, corrosion films, leached layers, and diffusion profiles
- In-depth concentration profiles of low-level dopants ($\leq$1000 ppm) diffused or ion implanted in semiconductor materials
- Hydrogen concentration and in-depth profiles in embrittled metal alloys, vapor-deposited thin films, hydrated glasses, and minerals
- Quantitative analysis of trace elements in solids
- Isotopic abundances in geological and lunar samples
- Tracer studies (for example, diffusion and oxidation) using isotope-enriched source materials
- Phase distribution in geologic minerals, multiphase ceramics, and metals
- Second-phase distribution due to grain-boundary segregation, internal oxidation, or precipitation

Samples

- *Form*: Crystalline or noncrystalline solids, solids with modified surfaces, or substrates with deposited thin films or coatings; flat, smooth surfaces are desired; powders must be pressed into a soft metal foil (for example, indium) or compacted into a pellet
- *Size*: Variable, but typically 1 cm × 1 cm × 1 mm
- *Preparation*: None for surface or in-depth analysis; polishing for microstructural or trace element analysis

Limitations

- Analysis is destructive
- Qualitative and quantitative analyses are complicated by wide variation in detection sensitivity from element to element and from sample matrix to sample matrix
- The quality of the analysis (precision, accuracy, sensitivity, and so on) is a strong function of the instrument design and the operating parameters for each analysis

Estimated Analysis Time

- One to a few hours per sample

Capabilities of Related Techniques

- *Auger electron spectroscopy*: Qualitative and quantitative elemental surface and in-depth analysis is straightforward, but the detection sensitivity is limited to >1000 ppm; microchemical analysis with spatial resolution to <100 nm
- *Rutherford backscattering spectroscopy*: Nondestructive elemental in-depth profiling; quantitative determination of film thickness and stoichiometry
- *Electron microprobe analysis*: Quantitative elemental analysis and imaging with depth resolution $\geq$1 μm

Introduction

In secondary ion mass spectroscopy (SIMS), an energetic beam of focused ions is directed at the sample surface in a high or ultrahigh vacuum (UHV) environment. The transfer of momentum from the impinging primary ions to the sample surface causes sputtering of surface atoms and molecules. Some of the sputtered species are ejected with positive or negative charges; these are termed secondary ions. The secondary ions are then mass analyzed using a double-focusing mass spectrometer or an energy-filtered quadrupole mass spectrometer. The principles of SIMS are represented schematically in Fig. 1.

This method can be used to acquire a variety of information about the surface, near-surface, or bulk composition of the sample, depending on the instrumental parameters. If the rate of sputtering is relatively low, a complete mass spectrum can be recorded to provide a surface analysis of the outermost 5 nm of the sample. This is often termed static SIMS. Although a useful mode of operation, it is not yet a routine analytical technique. Alternatively, the intensity of one or more of the peaks in the mass spectrum can be continuously recorded at a higher sputtering rate to provide an in-depth concentration profile of the near-surface region. At very high sputtering rates, trace element or impurity analysis in the bulk is possible. Finally, a secondary ion image of the surface can be generated to provide a spatially resolved analysis of the surface, near surface, or bulk of the solid. This article will focus on the principles and applications of high sputter rate dynamic SIMS for depth profiling and bulk impurity analysis.

In general, secondary ion mass spectroscopy can provide characterization of solid samples with high spatial and in-depth resolution; due to the inherent sensitivity of mass spectroscopy, this is usually attained with high detection sensitivity as well. The extent to which these capabilities can be realized, especially in a quantitative fashion, depends on the nature of the specimen, the instrument design, and the particular instrumental parameters and methods used in the analysis. The interpretation of SIMS spectra and depth profiles can be difficult; thus, SIMS is not yet applicable for chemical analysis of unknowns in the true sense of the word. Rather, SIMS has unique capabilities for answering specific questions about specimens whose stoichiometry and matrix structure are already characterized.

Sputtering

The bombardment of a solid surface with a flux of energetic particles can cause the ejection of atomic species. This process is termed sputtering (Ref 1-3), and in a more macroscopic sense, it causes erosion or etching of the solid. The incident projectiles are often ions, because this facilitates production of an intense flux of energetic particles that can be focused into a directed beam; therefore, these techniques are referred to as ion sputtering and ion beam sputtering. However, in principle, sputtering (and secondary ion emission) will also occur under neutral beam bombardment. Secondary ion mass spectroscopy is typically based on ion beam sputtering of the sample surface, although new approaches to SIMS based on fast atom bombardment are being developed.

The interaction between the energetic primary ions and the solid surface is complex. At incident ion energies from 1 to 20 keV, the most important interaction is momentum transfer from the incident ion to the target atoms. This occurs because the primary ion penetrates the solid surface, travels some distance (termed the mean free path), then collides with a target atom. Figure 2 shows schematically that this collision displaces the target atom from its lattice site, where it collides with a neighboring atom that in turn collides with its neighbor. This succession of binary collisions, termed a collision cascade, continues until the energy transfer is insufficient to displace target atoms from their lattice positions.

The sputtering, or ejection, of target atoms and molecules occurs because much of the momentum transfer is redirected toward the surface by the recoil of the target atoms within the collision cascade. Because the lifetime of the collision cascade produced by a single primary ion is much smaller than the frequency of primary ion impingements (even at the highest primary ion beam current densities), this process can be viewed as an isolated, albeit dynamic, event. The ejection of target atoms due to a single binary collision between the primary ion and a surface atom occurs infrequently.

The primary ion undergoes a continuous energy loss due to momentum transfer, and to the electronic excitation of target atoms. Thus, the primary ion is eventually implanted tens to hundreds of angstroms below the surface. In general, then, the ion bombardment of a solid surface leads not only to sputtering, but also to electronic excitation, ion implantation, and lattice damage. Figure 3 summarizes the effects of ion bombardment and indicates that the sputtered species may be monatomic species or molecular clusters. The effects of ion implantation and electronic excitation on the charge of the sputtered species are discussed in the section "Secondary Ion Emission" in this article.

The sputtering yield, S, is the average number of atoms sputtered per incident pri-

Fig. 1 Schematic representation of the principles of SIMS

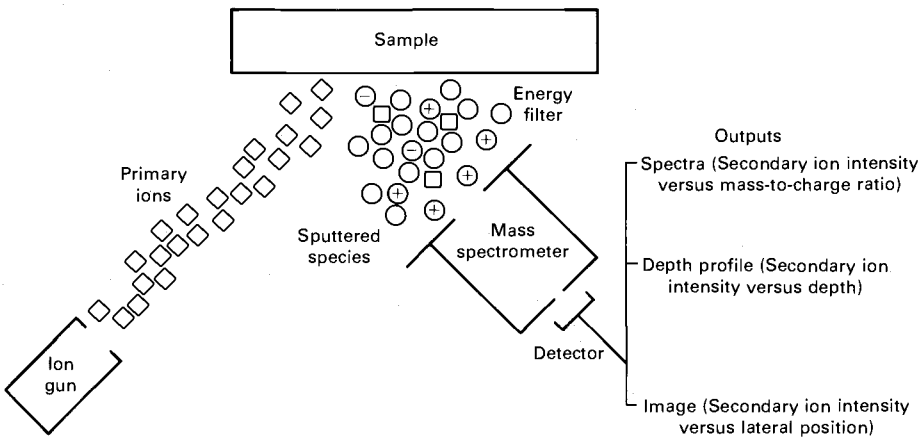

Fig. 2 The physical effects of primary ion bombardment: implantation and sputtering

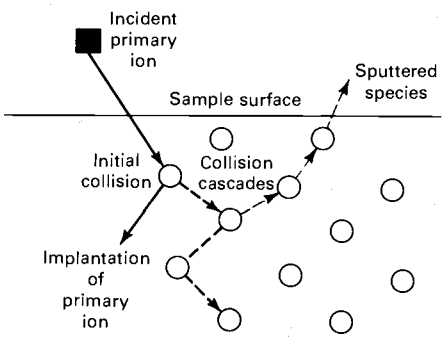

Fig. 3 Schematic diagram of the sputtered species ejected during primary ion bombardment of a compound $i_x j_y$

These sputtered species may be monatomic, molecular, and/or incorporate implanted primary ions. i = ○, j = ●

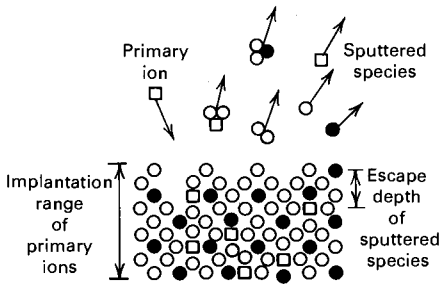

mary ion. This number depends on the target material and on the nature, energy, and angle of incidence of the primary ion beam. The sputtering yield is directly proportional to the stopping power of the target (because this determines the extent of momentum transfer near the surface), and it is inversely proportional to the binding energy of the surface atoms. Therefore, the sputtering yield also exhibits a dependence upon the crystallographic orientation of the material being sputtered. The sputter yield is usually assumed to be proportional to the square root of the incident ion energy, but there is not universal agreement with experiments in the energy range from 1 to 20 keV. In most SIMS experiments, Cs^+, O_2^+, O^-, and Ar^+ primary ion species are used in the energy range from 2 to 20 keV at angles of incidence between 45° and 90°. Under these conditions, the sputtering yields for most materials range from 1 to 20. Information on the effects of the primary ion beam and the target material on sputtering yields is provided in Ref 4.

Selective sputtering, or preferential sputtering, can occur in multicomponent, multiphase, or polycrystalline materials. Thus, it is possible for the composition of alloy surfaces to become modified during sputtering where the species with the lowest sputtering yield become enriched in the outermost monolayer, while the species with the highest yield are depleted. In the case of multiphase materials, those phases with the higher yield will be preferentially etched; this alters the phase composition at the surface, and introduces microtopography and roughness. For polycrystalline materials, the variation in sputter yield with crystallographic orientation can also lead to the generation of surface roughness during sputtering. All of these effects can influence the quality and interpretation of a SIMS analysis.

Secondary Ion Emission

The species ejected from a surface during sputtering may be monatomic, polyatomic, or multicomponent, and each of these may be positively charged (+), negatively charged (−), multiply charged (+p, −p), or neutral (0). Thus, the sputtering yield S for a compound of composition $i_x j_y$ can be expanded to:

$$S = \{(i^+) + (j^+) + (i^-) + (j^-) + (i_2^+) + (j_2^+) + (i_2^-) + (j_2^-) + (i^{2+}) + (j^{2+}) \ldots (i_n^{\pm p}) + (j_n^{\pm p}) + (i_2 j^+) + (i_2 j^-) \ldots + (i_n j_m^{\pm p}) + (i^0) + (j^0) + (ij^0) \ldots + (i_n^0)(j_n^0)(i_n j_m^0)\} \div I_p \quad \text{(Eq 1)}$$

where ( ) represent the fluxes of secondary ions and neutrals, and I_p represents the primary ion (or neutral) beam flux.

Whereas the sputter yield, S, defines the total number of species ejected per incident ion, the secondary ion yield, $S_{i_n}^{\pm p}$ defines the number of positive ions i^+, i^{+2}, i_2^+, i_n^{+p}, or negative ions, i^-, i^{-2}, i_2^-, i_n^{-p}, and in the case of multicomponent systems, molecular ions $i_n j_m^{+p}$ ejected per incident primary ion. It is related to the sputter yield, S, through a factor termed the ionization probability $\gamma_{i_n}^{+p}$; for example, in the case of material $i_x j_y$, one can define the secondary ion yield for i^+ as:

$$S_i^+ = \gamma_i^+ S(i_x j_y) \quad \text{(Eq 2)}$$

where γ_i^+ is the number of i^+ ions ejected divided by the total number of species ejected that contain i, and $S(i_x j_y)$ is the sputter yield for material $i_x j_y$.

The secondary ion yield is an important parameter because it determines the relative intensities of the various SIMS signals. The secondary ion yield depends on the same factors as the sputter yield, but it also depends on the ionization probability. Although a complete and unbiased theory of secondary ion emission, particularly the ionization probability, has not yet been reported, most models emphasize the importance of chemical and electronic effects (see the Selected References in this article). Accordingly, the presence of reactive species at the surface is believed to modify the work function, the electronic structure, and the chemical bonding, and all of these can influence the probability that a sputtered species will be ejected in a neutral or charged state.

The details of these various models are not important to this discussion. Rather, it is necessary to recognize that the secondary ion emission phenomenon is sensitive to the presence of electropositive or electronegative species at the sample surface. Thus, the sputtering of surfaces in the presence of oxygen enhances the production of many positive metal ions, because the electronegative oxygen increases the probability that the sputtered atom or molecule can release an electron. The oxygen may be a constituent of the sample (for example, a metal oxide), it may adsorb onto a metallic or semiconductor surface during the sputtering (for example, from an oxygen gas jet or a high residual oxygen pressure in the vacuum environment), or it may be implanted in the surface during the sputtering (for example, by using an oxygen primary ion beam). In all these cases, the production of positive ions is enhanced relative to that observed in the absence of the oxygen (or any other electronegative species); Table 1 shows the effect of oxygen on the absolute secondary ion yields of various metals. Similarly, the sputtering of surfaces in the presence of electropositive species (e.g., the use of Cs^+ primary ion beams) leads to an enhanced production of negative secondary ions.

There is an alternative to this chemical secondary ion emission mechanism. That is, in the case of very clean surfaces under inert ion bombardment in a UHV environment, intrinsic secondary ion emission may be observed. Under these conditions, the production of secondary ions is greatly reduced (Table 1, clean surfaces). However, this situation is seldom achieved in typical SIMS analyses because of the presence of reactive

Table 1 The effect of oxygen on positive secondary ion yields in metals

Element, M	Sputtering yield S_{M^+} (clean surface)	Sputtering yield S_{M^+} (oxygen-covered surface)
Magnesium	0.01	0.9
Aluminum	0.007	0.7
Titanium	0.0013	0.4
Vanadium	0.001	0.3
Chromium	0.0012	1.2
Manganese	0.0006	0.3
Iron	0.0015	0.35
Nickel	0.0006	0.045
Copper	0.0003	0.007
Strontium	0.0002	0.16
Niobium	0.0006	0.05
Molybdenum	0.00065	0.4
Barium	0.0002	0.03
Tantalum	0.00007	0.02
Tungsten	0.00009	0.035
Silicon	0.0084	0.58
Germanium	0.0044	0.02

Source: Ref 5

species in the specimen or vacuum environment, nor is it desirable, due to the need to enhance secondary ion production for detection sensitivity. Thus, intrinsic ion emission is of little concern here, because it contributes very little to the overall emission mechanism in conventional SIMS.

The secondary ion yield, which determines the measured SIMS signal, is a very sensitive function of the chemical and electronic properties of the surface under bombardment. Thus, it exhibits a dependence upon the element, its matrix, and the bombarding species being implanted in the surface during the analysis; moreover, it is influenced by residual gas pressure and composition during the analysis because adsorbates can modify the chemical and electronic state of the surface monolayer.

The matrix dependence of the secondary ion yield is the characteristic of secondary ion emission that has received perhaps the most attention. In the case of inert primary beam bombardment, for example, Ar^+ on aluminum versus aluminum oxide, the positive metal ion yield is recognized to be three to four orders of magnitude higher in metal oxides than in their pure metal counterparts. This ion yield dependence is due to the ionization probability, γ^+_{Al}, which is approximately 100 times greater for Al_2O_3 than for aluminum metal, not to the sputtering yield, which is approximately two times greater for the metal than for the metal oxide.

Similarly, Ar^+ bombardment of a pure aluminum metal sample is known to produce a larger Al^+ signal in a dirty vacuum or in the presence of an intentional oxygen leak than in a nonreactive UHV environment. Therefore, most modern approaches to SIMS analysis—at least when quantitative elemental analysis is of interest—use reactive primary ion beams rather than inert ion beams; an oxygen beam (O_2^+ or O^-) or a cesium (Cs^+) beam is typically used. Thus, the surface is always saturated with a reactive species (due to the primary ion implantation) that enhances the ion yield and makes the elemental analysis less sensitive to matrix effects and/or to the residual vacuum environment during analysis.

Crystallographic orientation further compounds the matrix dependence of the secondary ion yield. This is due primarily to the difference in electronic properties (for example, work function or band structure) from one crystal face to another and to the difference in adsorptivity or implantation range from one face to another (and much less so due to variation in sputtering yield). In the case of polycrystalline and/or multiphase materials, the emission intensity can vary considerably from one grain to another. This can be an important source of contrast in secondary ion emission imaging of polycrystalline materials.

Regarding the energy and angular distribution of the ejected species, the secondary ions are ejected with a wide distribution of energies. The distribution is usually peaked in the range from 1 to 10 eV, but depending on the identity, mass, and charge of the particular secondary ion, the form of the distribution will vary. In general, the monatomic species (for example, i^+ or j^+) have the widest distribution, often extending to 300 eV under typical conditions; the molecular species (such as i_2^+ or i_2j^+) cut off at lower energies. The energy distribution of the ejected secondary ions is relevant to the design of the SIMS instrument (because it must be energy filtered before mass analysis) and to the mode of operation (because i^+ can often be resolved, for example, from i_2^+ or j_2^+ on the basis of energy).

Instrumentation

There is a wide variety of instrument designs for SIMS, and the quality and applicability of the analysis depends strongly on the details of the instrumentation. Secondary ion mass spectroscopy instruments can be categorized into three broad classifications in which the distinctions refer to versatility, mass resolution, primary beam characteristics, and, in particular, imaging capability.

The simplest SIMS instrument, sometimes called an add-on, macro-, or broad-beam instrument, is intended primarily for surface analysis and qualitative depth profiling and less so for quantitative elemental analysis, microanalysis, or imaging. This is seldom a dedicated unit, but rather a set of components often used in conjunction with an Auger or x-ray photoelectron spectrometer. Figure 1 shows a simple SIMS system. The instrument uses a standard electron-impact inert ion gun that is often the same sputter gun used for sample cleaning or Auger sputter-profiling. The mass spectrometer is usually a quadrupole type, but to select a portion of the wide energy distribution of sputtered secondary ions, it requires an energy prefilter. Other than the addition of the energy prefilter, the quadrupole mass spectrometer and the ion detector are very standard.

A dedicated SIMS instrument often incorporates a more intense, finely focused primary ion beam suitable for probe imaging. Because it is unnecessary to provide the flexibility for performing analyses by Auger electron spectroscopy (AES) or x-ray photoelectron spectroscopy (XPS) in this type of instrument, the sample orientation and the ion collection system can also be optimized. These instruments, often called ion microprobes, are designed primarily for quantitative in-depth profiling and microanalysis and less so for surface analysis. Figure 4 shows a typical ion microprobe that uses a duoplasmatron ion source to generate inert, as well as reactive, primary ion beams. The instrument shown in Fig. 4 and most commercially available units use an energy-filtered quadrupole mass spectrometer, but in principle, a magnetic analyzer could also be used.

A direct-imaging SIMS instrument, usually called an ion microscope, creates a secondary beam with the ejected secondary ions. The secondary beam is mass analyzed in a double-focusing electrostatic/magnetic sector; the transmitted secondary ions can then be counted or used to create a direct image of the sample surface on a microchannel plate. Figure 5 shows a schematic diagram of a direct-imaging ion microscope in which the primary ion beam and secondary ion beam are clearly distinguished. This instrument is designed primarily for microstructural analysis and imaging, quantitative in-depth profiling, and trace element analysis. It is not suitable for true surface analysis, and due to the precise ion collection optics, the ability to treat or manipulate the specimen *in situ* is essentially lost.

System Components. The design and operation of the various instrumental components will not be discussed in detail, because many excellent treatments are available (Ref 6-8). However, there are several components and features of the instruments whose specific design and/or availability can influence the quality of the analysis. These are summarized below.

The quality of the vacuum environment during SIMS analysis is important for two reasons. First, any variations in the vacuum pressure can influence the secondary ion intensity due to the effects of reactive species on ionization probability and, to a lesser extent, on sputtering rate. Thus, day-to-day reproducibility and the quality of the depth profile, which must be acquired under constant vacuum pressure, will be affected. Second, the pressure and composition of the vacuum environment will influence the background levels and therefore the detection limits for some species. This is usually due to their adsorption onto the surface and their subsequent ejection as secondary ions. The background species of most concern are hydrogen, oxygen, and water, because these are readily adsorbed and quite prevalent in most vacuum systems. Ideally, pressure of the order of 10^{-9} to 10^{-10} torr should be maintained at the specimen surface, especially for hydrogen (Ref 9), oxygen, or carbon analysis.

Fig. 4 Schematic diagram of the layout and components used in an ion microprobe

Courtesy of ISA Inc., Riber Division

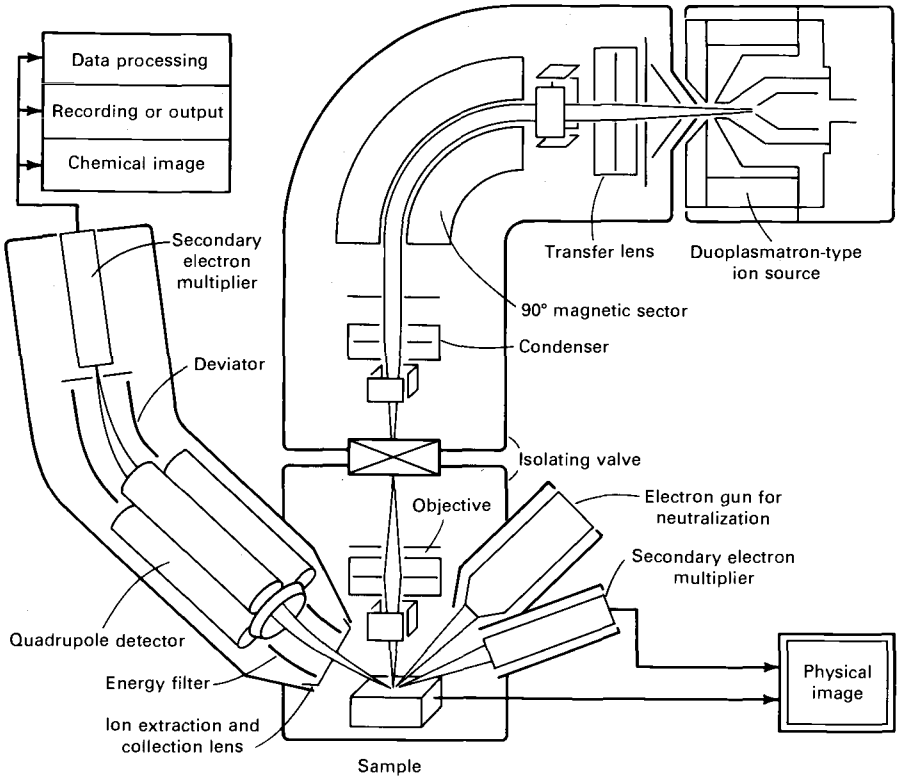

Fig. 5 Schematic diagram of the layout and components used in an ion microscope

Courtesy of Surface Science Western

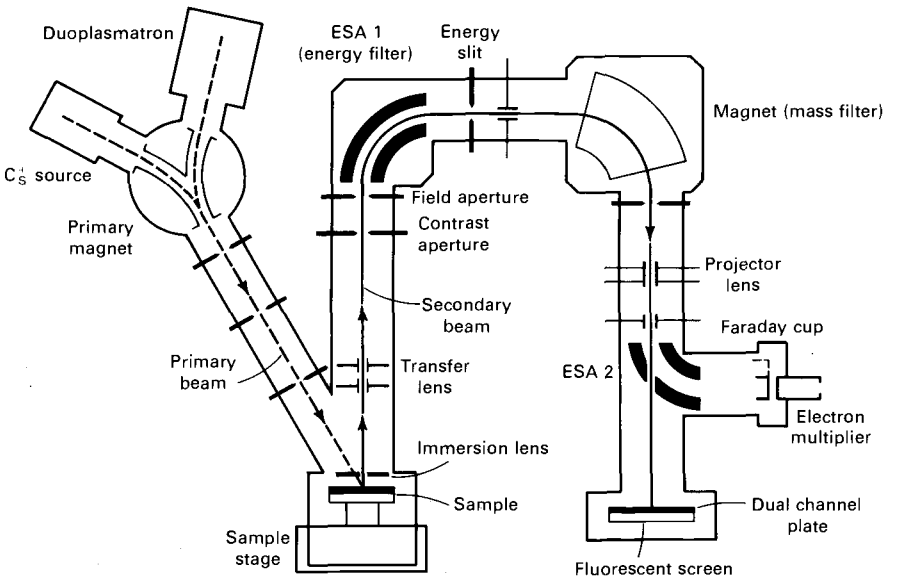

In the case of the primary ion beam, several features are of interest. First, the ability to generate reactive primary ions, for example, O_2^+ O^-, and Cs^+, requires a duoplasmatron or liquid metal source; the more conventional electron-impact ion guns typically used in surface analysis are limited to inert species (He^+, Ne^+, or Ar^+). The negative oxygen species can be of great benefit for the analysis of insulators. Second, the beam diameter and maximum current density characteristics will vary with the type and design of the gun. Simple ion guns usually provide beam diameters (spot sizes) of the order of 25 to 250 μm; dedicated ion microprobes and ion microscopes can produce spot sizes as small as 1 to 2 μm. Third, the background levels that can influence detection limits are controlled to some degree by the ion source. This refers not only to residual gases, but also to metallic species that can become incorporated in the beam, implanted in the sample, and then ultimately appear in the analysis of the sample.

The ability to pump the ion source differentially (relative to the sample chamber) can greatly alleviate the background due to residual gases and other contaminants produced in the ion source. However, the metallic and other impurities that become ionized and thus incorporated in the primary ion beam are most effectively eliminated using a primary beam mass filter, essentially a mass spectrometer that filters the primary ions before they strike the specimens. A primary beam mass filter will also reject any neutral species in the beam. The use of a primary beam mass filter is almost a necessity for trace element and low-level dopant analyses. Finally, rastering of the primary ion beam over the specimen surface is a requirement in SIMS depth profiling and secondary ion imaging; thus, incorporation of raster plates is now fairly standard in most ion guns and SIMS systems.

The secondary ion collection optics represent the feature that is perhaps most variable among commercial and laboratory-built SIMS systems. Ideally, the secondary ions are extracted electrostatically from the center of the crater (over the maximum solid angle), instead of simply collecting that portion of the ejected flux of secondary ions that intersects the entrance aperture of the analyzer. Many dedicated SIMS instruments include an extraction lens over the sample, but this limits the sample geometry that the instrument can tolerate and the capability for a multitechnique apparatus. The extracted secondary ions are then energy analyzed to select the optimum portion of the energy distribution for subsequent mass filtering; if this is not done, mass resolution is severely degraded. This is an absolute necessity for

quadrupole spectrometers and single-focusing magnetic sectors, whereas an electrostatic energy filter is an inherent component of higher resolution double-focusing magnetic mass spectrometers. Various electrostatic energy filters are available for use with quadrupoles, including grids, apertures, Bessel boxes, and spherical or hemispherical plates (Ref 10); the collection efficiency, selectivity, resolution, and transmission of these filters vary and will influence the overall sensitivity of the SIMS instrument.

The instrumental features required for secondary ion imaging are presented in the section "Ion Imaging" in this article, while the differences between quadrupole and high-resolution magnetic mass filters are described in the next section of this article. Data acquisition for spectral and depth-profiling analyses simply requires an ion detector and an automated control for scanning the mass spectrum or, in the case of depth profiling, for sequential acquisition of selected peak intensities in the spectrum. The ion detector should be electronically gated in all instruments except the ion microscope, in which apertures can be used to eliminate crater-edge effects. The instrumental features for computerized data acquisition, data manipulation, and output vary considerably, depending on the versatility of the mass spectrometer.

Secondary Ion Mass Spectra

Figure 6 shows the positive SIMS spectrum for a very high purity silicon sample (Ref 11). This bar graph was obtained in an ion microscope using an O_2^+ primary ion beam and a double-focusing mass spectrometer. The spectrum shows the presence of silicon isotopes $^{28}Si^+$, $^{29}Si^+$, and $^{30}Si^+$ and thus demonstrates the isotopic sensitivity of SIMS. Also shown are the polyatomic species Si_2^+ and Si_3^+ and the molecular species SiO^+, SiO_2^+ Si_2O^+, $Si_2O_2^+$ Si_3O^+, $Si_3O_2^+$ $Si_3O_3^+$ and so on. In this case, the oxide species are not representative of the silicon sample, but are due to the use of the oxygen primary beam. The oxygen ions are implanted in the surface, and these charged molecular secondary ion clusters are subsequently sputter-ejected. In addition, of course, the $^{16}O^+$ and $^{32}O_2^+$ secondary ions are also generated.

The use of an oxygen primary ion beam has enhanced the positive secondary ion yields; therefore, the measured secondary ion signals are quite strong. If this specimen had been analyzed using an inert primary ion beam (for example, argon), the positive secondary ion signal intensities would be 100 to 1000 times less intense, and the presence of the aluminum impurity ($^{27}Al^+$) probably would not have been detected. In some instances, it may be considered a disadvantage to use an oxygen primary beam for enhancing the secondary ion yields, because it precludes an oxygen analysis in the specimen. However, it is common to use an ^{18}O primary ion beam when ^{16}O analyses are of interest or to use a Cs^+ beam (if available), because it enhances the secondary ion yield for electronegative species such as oxygen.

The other peaks in the spectrum shown in Fig. 6 that have not been identified are due primarily to the molecular species that form between the silicon sample and implanted primary ions as well as between the Si_n, O_n, Si_nO_m species and ^1H, ^{12}C, and ^{14}N in the residual vacuum. The SIMS spectrum is clearly very complex due to this multitude of molecular secondary ion matrix species. Although it may not be evident in this bar graph (Fig. 6), the presence of the molecular species further complicates the analysis due to mass interferences. For example, Si_2^+ (m/e = 55.9539) will interfere with Fe^+ (m/e = 55.9349) unless the spectrometer is optimized for and capable of high resolution (m/e is the mass-to-charge ratio).

The interference problem and spectral complexity become even more evident in multicomponent specimens. Figure 7 shows portions of the SIMS spectra for a stainless steel. The molecular secondary ions from the matrix species (Fig. 7a) represent a background that precludes identification of minor or trace elements in this material. Figure 7(b) shows that much of this background can be eliminated by energy-filtering the secondary ions; here, only the higher energy secondary ions, dominated by the monatomic species, are permitted to enter the mass analyzer.

The advantages of a selective energy filter and a high mass resolution spectrometer are further demonstrated in Fig. 8. This CuTi specimen produced a doublet at mass number 63 that could be resolved to show the presence of both Cu^+ (m/e = 62.9296) and TiO^+ (m/e = 62.9467) secondary ions. The spectra shown in Fig. 8 demonstrate the detection sensitivity and resolution that can be achieved in a double-focusing magnetic spectrometer by energy filtering and high-resolution mass filtering; this is 10 to 100 times the resolution obtainable with a quadrupole spectrometer.

The spectra shown in Fig. 6 to 8 really represent the bulk composition of these samples. This is due in part to the nature of the specimens, which were not subjected to any surface treatment, but it is also a result of the analysis mode. The use of an oxygen (or any reactive) primary ion beam requires the attainment of a steady state in the surface and the detected signal. During this transient time period, the reactive primary ions are implanted in the surface up to a steady-state concentration determined by the primary beam energy and flux, the target material, and the total sputtering rate. The ion yields are changing during this period; therefore, the SIMS spectra generated during the first few minutes of sputtering (in the outermost 10 to 20 nm) are of little analytical value. Moreover, the ability to detect very low concentration levels requires the use of high sputtering rates when data acquisition in the surface would be difficult even in the absence of the transient effect. Clearly, then, the data in Fig. 6 to 8 represent trace element analyses in the near surface or bulk, not true surface analyses.

Fig. 6 Positive SIMS spectra (in the form of a bar graph) for high-purity silicon under oxygen bombardment in an ion microscope

Source: Ref 10

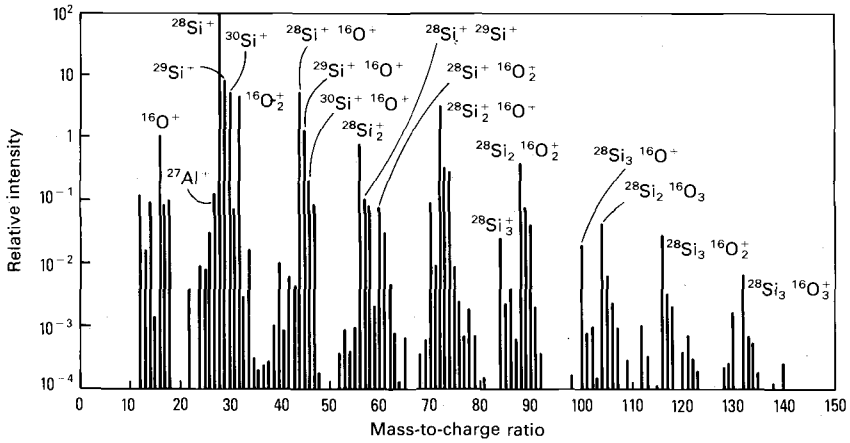

Fig. 7 Positive SIMS spectra for an NBS reference steel under oxygen bombardment in an ion microscope

(a) Recorded without a voltage offset. (b) Recorded with a voltage offset to reject low-energy molecular secondary ions

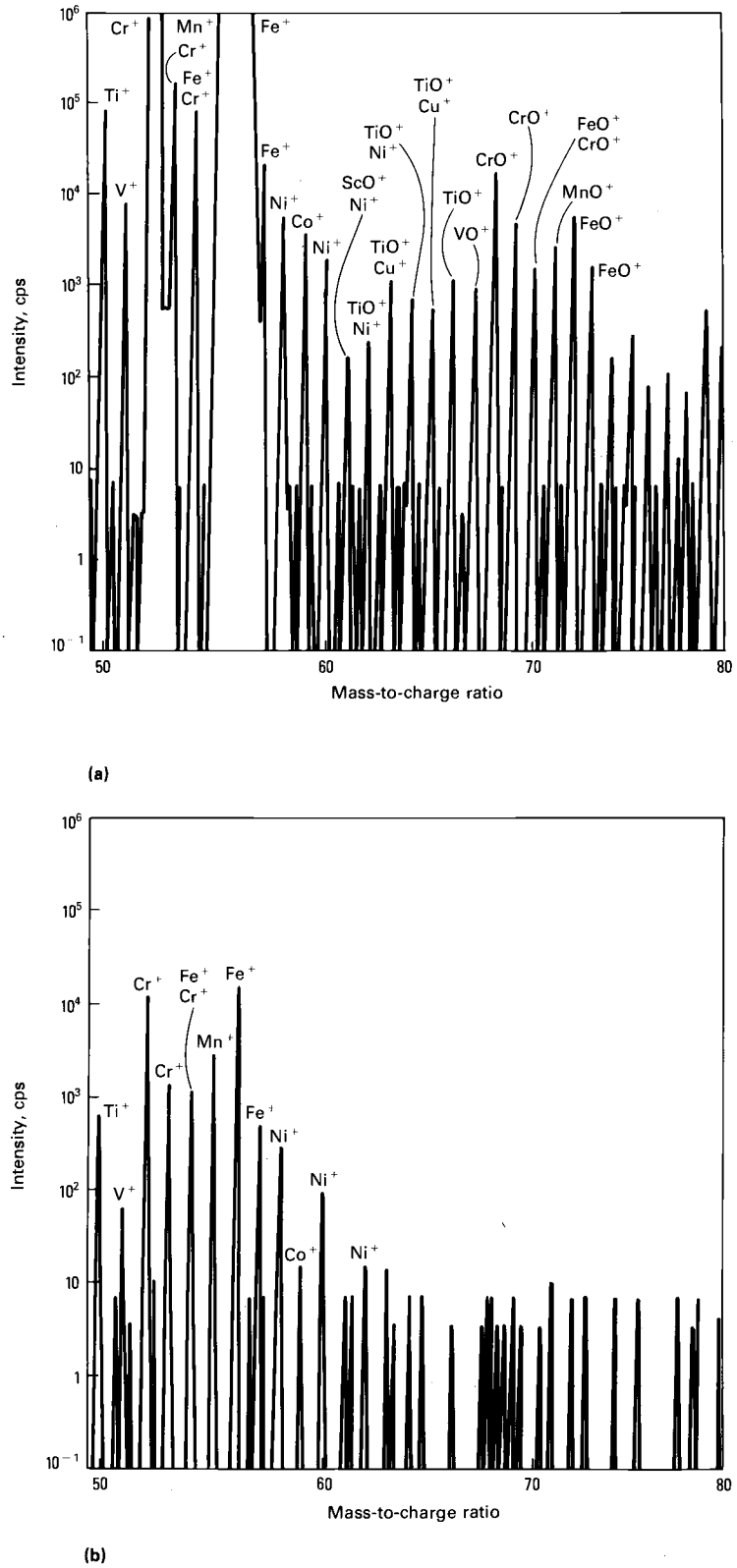

Fig. 8 High-resolution mass scan over the region of *m/e* = 63 for a CuTi specimen

Obtained using an ion microscope

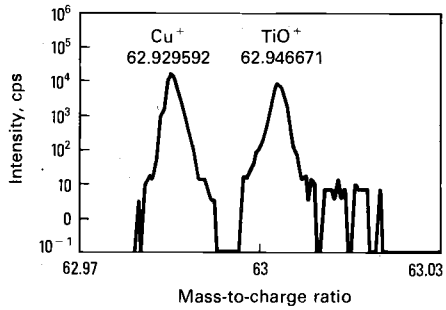

Figure 9 presents the positive SIMS spectrum for a silicon substrate upon which an organometallic silicate film (~100 nm thick) has been deposited. In contrast to the spectra shown in Fig. 6 to 8, this spectrum was obtained in an ion microprobe using an argon primary ion beam and an energy-filtered quadrupole mass spectrometer. Due to the oxide nature of the film, the ion yields are more than sufficient to produce measurable intensities, even though an inert argon primary ion beam is used. Because the spectrum is presented on a linear scale, much of the background due to the molecular secondary ions has been eliminated.

The spectrum indicates the presence of hydrogen and hydroxylated molecular oxide species, but the quadrupole analyzer has insufficient resolution to separate the interferences. Although some of these molecular species may be due to hydrogen background in the vacuum system, they are primarily indicative of the hydrated nature of the film. There also appear to be boron, carbon, sodium, and potassium impurities in the film. These impurities were undetected in a corresponding Auger analysis; thus, the high sensitivity of SIMS is further exemplified. This spectrum demonstrates the use of SIMS for a thin film analysis, in this case using an inert primary ion beam. In the next section in this article, a depth profile will be presented for this film that demonstrates the effects of the matrix change (at the oxide film/semiconductor substrate interface). The in-depth analysis of oxide and other nonmetallic films and coatings on metallic or semiconducting substrates is a common objective of SIMS analyses in metallurgy and materials science.

Due to the high detection sensitivity in SIMS, almost any constituent can be found in the SIMS spectrum. The analyst must determine (1) whether or not these constituents are inherent to the sample or to the instrument background and (2) what concen-

Fig. 9 Positive SIMS spectra for an organometallic silicate film deposited on a silicon substrate

Obtained using a scanning ion microprobe under inert argon bombardment

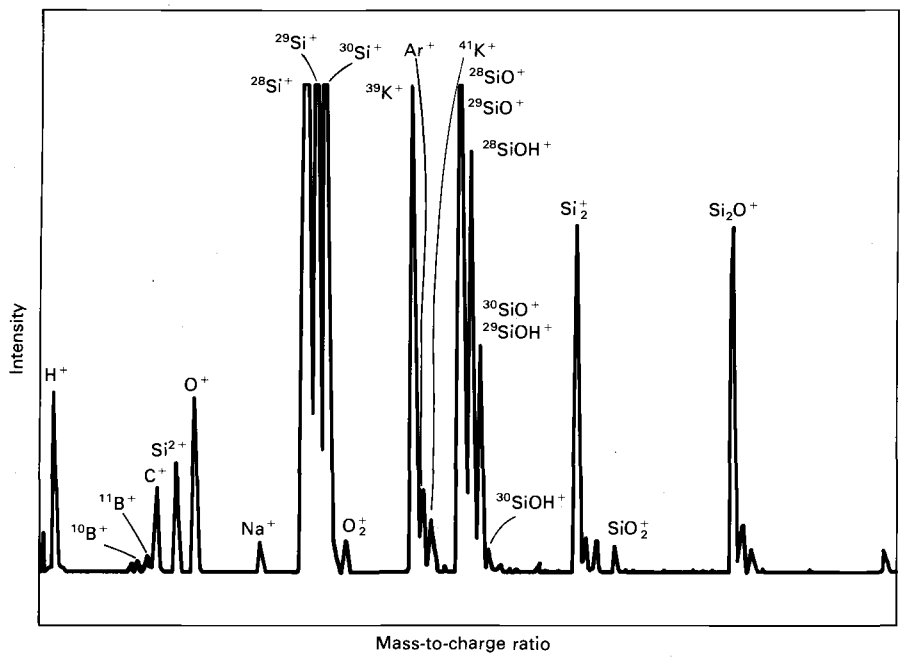

Fig. 10 Depth profiles for the organometallic silicate film shown in Fig. 9

Note the matrix effects at the film/silicon substrate interface due to the use of an inert argon ion beam. Obtained using raster gating in a scanning ion microprobe

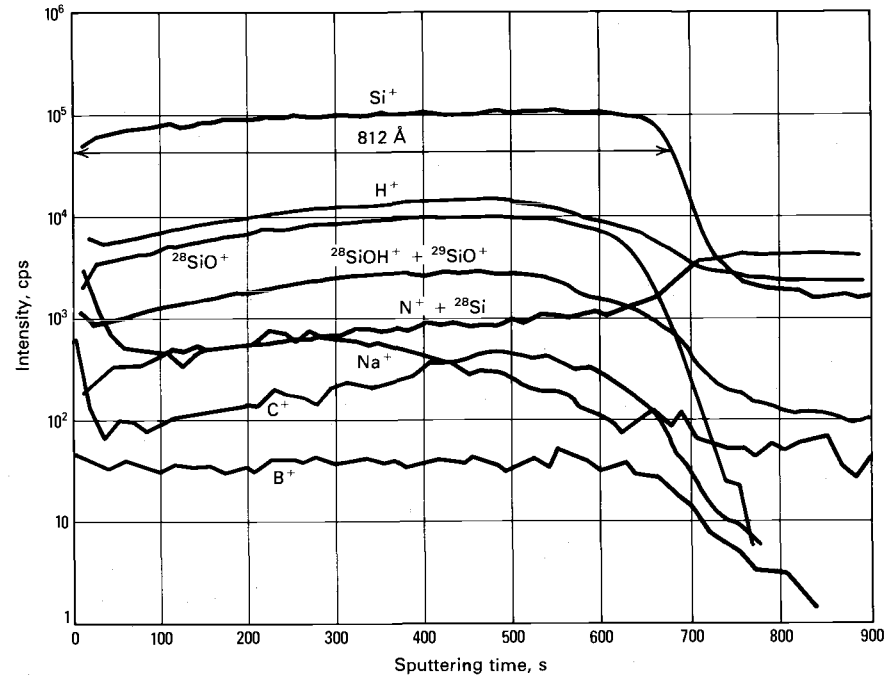

tration levels the peak intensity represents. Thus, even qualitative analysis with SIMS is a nontrivial matter, because the presence of certain species in the spectra may be independent of the sample and/or may be at levels that are negligible relative to the problem.

Depth Profiles

As noted above, with the exception of static SIMS, most analytical applications of SIMS do not emphasize true surface compositional analysis. Rather, in-depth profiling (from 20 to 2000 nm), bulk impurity analysis, and imaging of microstructural features are more common applications of SIMS. Of these, quantitative depth profiling with high detection sensitivity and depth resolution is unquestionably the forte of SIMS. In a depth-profiling analysis, one or more of the secondary ion signals are monitored as a function of sputtering time (or depth) into the surface or bulk of the specimen or through an adherent thin film or coating.

The profiles shown in Fig. 10 illustrate several important points about matrix effects and the use of reactive primary ion beams in thin film profiling. These profiles were obtained for the film whose spectrum is shown in Fig. 9. The interface between the silicate film and silicon substrate is evident. This is due to the change in secondary ion yield between the oxide thin film and the silicon substrate. Although the substrate is pure silicon, the $^{28}Si^+$ signal falls by nearly two orders of magnitude between the film and substrate. In contrast, although the effects are fundamentally related, the $^{28}Si^{2+}$ signal increases by a factor of ten upon sputtering through to the substrate. These are matrix effects upon the secondary ion yields (or, more specifically, the ionization probability), not indications of any concentration or chemical structure change at the interface. If an oxygen primary ion were used in this analysis, the changes in secondary ion signal for $^{28}Si^+$ and $^{28}S^{2+}$ would not occur (at least under ideal conditions), although a transient would be observed in the signals at the interface (during which time the oxygen primary ion implantation would reach a steady state). Clearly, the use of an inert primary beam enhanced location of the film/substrate interface.

There are advantages to be gained in using an oxygen primary ion beam for a depth-profiling analysis of this type. They have little to do with the silicon species as such, but rather concern the interpretation of the other signals. For example, the $^1H^+$, $^{12}C^+$, $^{23}Na^+$, and $^{11}B^+$ signals also drop at the interface. However, the extent to which the signal drop is due to the matrix effect versus

any real change in concentration is unknown. Due to the large variation in ionization between the oxide film and semiconducting substrate, the concentrations of hydrogen, carbon, sodium, and boron could increase, even though their signals decrease. The use of a reactive primary ion beam would be of great benefit in this situation. The oxygen implantation would in this case provide a constant matrix from which the secondary emission could occur throughout the depth-profiling analysis. Therefore, any changes in these signals would be due to real concentration gradients. Thus, it would be possible to follow the B^+, Na^+, or H^+ across the interface to follow, for example, diffusion effects.

In addition to the minimization of matrix effects, the use of a reactive oxygen primary ion beam would also enhance the sensitivity (or detectability) for positive ions in the silicon substrate. This effect is perhaps best exemplified in Fig. 11, which shows a depth profile for boron in silicon (the quantitative analysis of which will be discussed in the next section of this article). The boron is a dopant that was intentionally put into the surface of this sample by ion implantation. The profile was obtained using an oxygen primary ion beam. These levels of boron could not be detected under argon bombardment (nor with AES or XPS); the yield enhancement due to the use of a reactive primary ion beam is critical to this analysis. In addition, the $^{30}S^{2+}$ matrix signal did not vary over the profile; that is, the observed variation in the boron signal is due to a real change in concentration.

The factors that determine or influence the depth and interface resolution of the measured profiles must now be considered. This complex subject has received considerable attention because it is depth profiling with high resolution for which SIMS is most applicable and unique. Discussions of SIMS depth profiling more detailed than that presented below are provided in the Selected References.

A depth-profiling analysis aims to define the concentration or concentration gradient of selected elements at finite depths below the original surface. Thus, the detected secondary ion signal must originate from well-defined planes below and parallel to the original surface. Ideally, these planes would be of atomic dimensions (in which case the in-depth resolution would be atomic or monomolecular), but Fig. 3 illustrates that the ejected secondary ions originate from a layer with a finite thickness termed the escape depth.

The escape depth varies to some extent with the energy and mass of the primary ions as well as with the material, but it is typically 3 to 5 atomic layers. In practice, though, this theoretical limit on depth resolution is not achieved. At the very least, each composition or concentration data point defined in the depth profile requires the erosion of sufficient material to collect a measurable and statistically significant secondary ion signal; this effective layer thickness depends on the sputtering rate and the secondary ion yield.

Perhaps of greater concern are a number of other phenomena, including crater-edge effects, halo effects, knock-on, atomic mixing, diffusion, preferential sputtering, and roughening, which are essentially artifacts that distort the true profile. Some of these effects are instrumental and can be alleviated to some extent through the design of the apparatus, but others are intrinsic to the sputtering process. Altogether, these effects can limit the depth resolution in a typical SIMS depth-profiling analysis from the theoretical limit of approximately 1 nm to as much as 5 to 10 nm. Thus, special attention should be paid to the effects described below when the highest possible depth resolution is required.

Figure 12 shows a schematic cross section through a sample that has a distinct surface layer. For the purposes of this discussion, it will be assumed that the layer is approximately 1 μm thick and that the interface between the layer and substrate is atomically sharp (the latter is unlikely in practice, but the assumption allows defining the extent to which the SIMS measurement itself broadens the true interface). Again, this schematic sample design represents a common situation that can arise in practice by oxidation, nitridation, or other surface treatment of a metal or semiconductor, or by deposition of thin films and coatings by one of a multitude of techniques. Although a SIMS analysis could be used to determine the composition or compositional uniformity of the layer, it would more likely be applied to answer the following questions:

- What impurities are present in the layer, and what are their concentration and depth distribution?
- What are the thickness of the film and the width of the interface?
- What is the diffusion profile for selected surface or interfacial reactants?
- Has segregation or compound formation occurred at the interface?

The effects to be described below can influence any depth-profiling analysis, regardless of the presence or absence of a distinct surface layer, but consideration of a surface film of finite thickness with a subsurface interface best illustrates the points.

A situation that can be most detrimental to depth resolution is shown in Fig. 12(b). This crater-edge effect is the result of nonuniform erosion of the specimen caused by nonuniform distribution of ions in the primary beam. The detection system will simultaneously filter and count secondary ions

Fig. 11(a) Raw $^{11}B^+$ and $^{30}Si^{2+}$ secondary ion signals versus sputtering time for a boron-implanted silicon substrate

Obtained using oxygen beam bombardment in an ion microscope

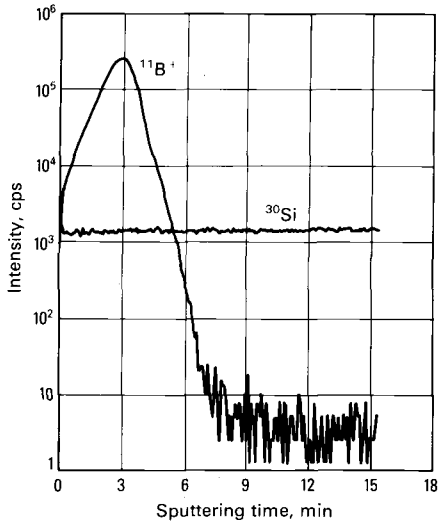

Fig. 11(b) Boron profile (see Fig. 11a) after quantitative analysis of the sputtering rate and secondary ion intensity

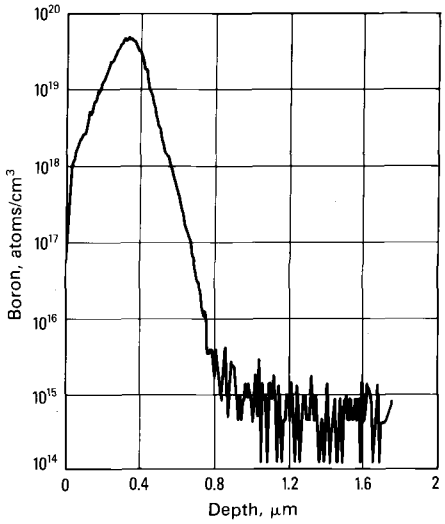

Fig. 12 Schematic representations of the artifacts that can distort a SIMS depth-profiling analysis

See text for details.

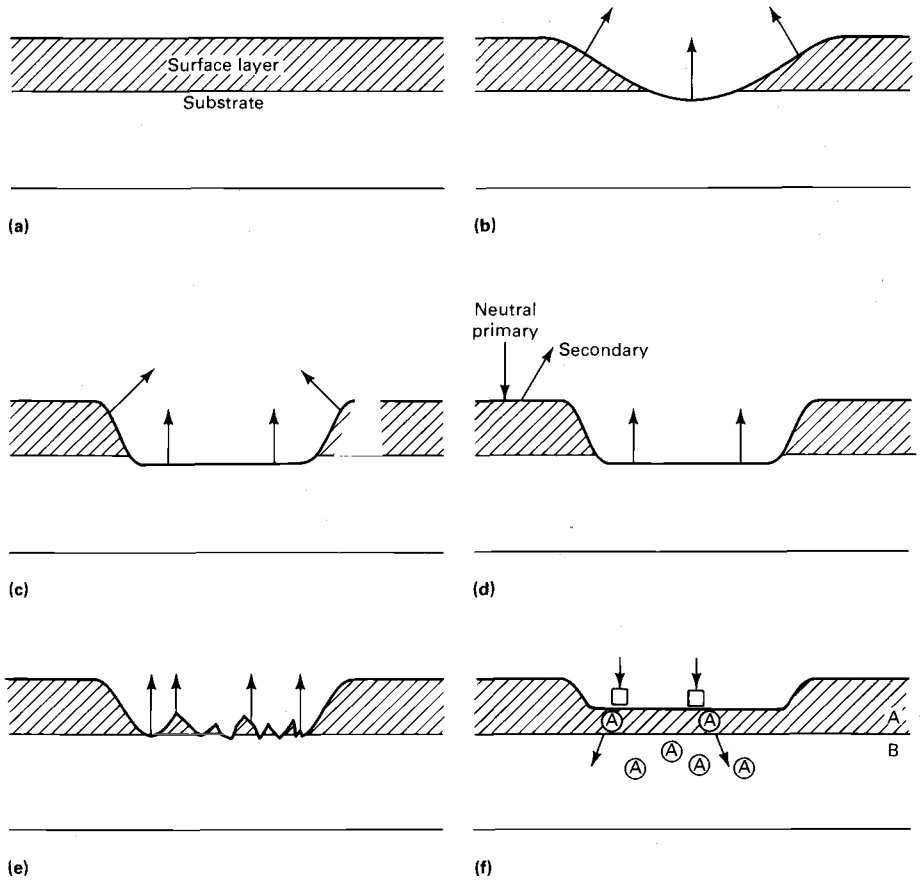

over a range of depths in the sample, and the depth resolution will be severely degraded. The practical consequence of this in the measured depth profile is a gross broadening of interfaces, diffusion profiles, or surface layer thicknesses. The most common remedy is to produce a flat-bottomed crater (Fig. 12c) by rastering a focused ion beam in a square pattern over the specimen. In this case, most of the secondary ions originate from a well-defined depth, but there are still contributions from the side walls.

There are several approaches to eliminating side-wall contributions, which may seem negligible but which nonetheless can limit depth resolution. In simple SIMS systems and ion microprobes, electronic raster gating is used. In this method, the scanning primary ion beam and the detector are synchronized so that whenever the ion beam is near the periphery of the crater, the collected secondary ions are not counted. Under optimal conditions, secondary ions would be detected only from the central 10 to 20% of the crater; obviously, the electronic rejection of 80 to 90% of the secondary ions reduces the signal and thus the detection limits. However, this is an absolute requirement for the acquisition of meaningful depth profiles. In the ion microscope, the direct-imaging optics preclude the need for electronic gating, because the extraction lens and field aperture combine to gate off the side-wall contributions mechanically.

The mechanical aperture used in the ion microscope has an additional advantage over electronic raster gating because it can reject secondary ions produced by neutral primary species bombarding the specimen. That is, the primary ion beam will contain a neutral component of energetic species (unless the primary beam is electrostatically deflected before striking the specimen) that does not respond to the raster plates. Thus, as shown in Fig. 12(d), there can be secondary ion ejection and detection from the original surface (and side walls) regardless of the position of the primary ion beam. The analysis will show species that may be present only near the original surface even when the erosion has proceeded to great depths; in this situation, species present only at the original surface or in the overlayer can be mistakenly believed to have migrated or diffused deep into the specimen. A useful remedy for this (when direct-imaging ion microscopy is not available or is ineffective) is to coat the specimen with a thin film of gold or other material that is not expected to be found in the specimen during analysis.

Figure 12(e) describes another effect that must be recognized in the interpretation of depth profiles. The ion beam erosion of even atomically smooth, single-crystal materials can generate roughness, but in polycrystalline or multiphase materials, this roughening can be especially severe due to differential sputtering rates (from grain to grain or phase to phase). This too will broaden the appearance of interface or diffusion profiles. The scale of the roughness increases with sputtering time and is usually assumed to be approximately 10% of the etch depth plus the original roughness. For example, after sputtering a smooth single crystal to a depth of 1 μm, the scale of the roughness is approximately 100 nm, and even an atomically sharp interface encountered at that depth will appear to be approximately 100 nm in width.

Figure 12(f) depicts a phenomenon termed atomic mixing or knock-on. Here, the primary ions displace atoms, for example, across an interface, and thus distort their original distribution. This effect can be minimized to some extent by using primary ions with lower energy and higher mass. Another related source of distortion is beam-induced diffusion or migration of solute species due to heating, radiation damage, chemical interaction with implanted primary ions, and electrostatic charging of the surface. In some cases, these effects cannot be avoided, and caution is advised.

There is at least one other source of distortion in a depth profile. It occurs only in multicomponent materials due to a phenomenon termed preferential sputtering. This is a transient effect that occurs at the beginning of a depth profile (or at internal interfaces) due to differences in sputtering yield among the various constituents.

This preferential sputtering effect in, for example, alloy *AB* changes the relative concentration of *AB* in the sputtered surface region so that the concentration of the high-yield species is reduced, and the concentration of the low-yield species is enhanced. Thus, once the transient is complete, the steady-state sputtered surface composition yields a relative flux of secondary ions *A* and *B* that is proportional to their true concentration ratio in the material. That is, in a sample where $S_A \neq S_B$, the relative fluxes of *A* and *B*

do not represent their true concentration ratio until preferential sputtering has occurred.

In a SIMS analysis, then, the relative secondary ion signals can change even in the absence of a true concentration gradient in the material. This transient will persist only over a short range (of the order of 1 to 10 nm) and thus is another reason to ignore the first portion of the depth profile. Nonetheless, it can be a severe limitation for the surface analysis of metal alloys or for the analysis of interfaces between alloy films.

An important parameter required for the interpretation of depth profiles is the sputtering rate. These rates typically range from 0.5 to 50 nm/min and are fundamentally related to the incident ion current density at the sample surface and the sputter yield of the material for the type and energy of the primary ions being used. In practice, the sputter rate is determined for a given set of operating conditions and the material of interest by measuring the depth of the sputtered crater. The crater depth can be measured using optical interferometry or profilometry. When appropriate, the sputter rate can also be obtained by depth profiling films of known thicknesses; that is, thin films whose thicknesses have been measured independently using optical techniques or Rutherford backscattering spectrometry (RBS). In this case, it must be assumed that the sputtering rate of the film will be the same as that of the specimen. Therefore, the use of oxide or metallic films for the determination of sputtering rates of bulk materials—even if the film and the bulk are of identical composition—is not recommended.

In general, it is not necessary to measure the sputter rate for each analysis of the same material if the primary ion beam current can be accurately measured or reproduced. In some cases, it is possible to translate the sputtering rate measured for one material into a rate appropriate for another material using tabulated values of the sputter yield. However, the sputtering rate can vary through a depth profile where large concentration changes occur; that is, it is an assumption to apply a constant sputtering rate to a depth profile if the concentration or composition changes are severe.

Quantitative Analysis

The relationship between the secondary ion current I_i^+ (that is, the positive secondary ion count rate for a monoisotopic element i) and the concentration of i in the specimen is:

$$I_i^+ = I_p \cdot S \cdot \gamma_i^+ \cdot C_i \cdot \eta \qquad \text{(Eq 3)}$$

where I_p is the primary ion beam current, S is the sputter yield, γ_i^+ is the ionization efficiency for i^+, C_i is the atomic fraction of i, and η is an instrumental factor that characterizes the collection, transmission, and detection efficiency of the instrument, that is, the ratio of ions i^+ emitted to ions i^+ detected. Clearly, the problem in quantitative SIMS analysis is that the measured signal I_i^+ depends not only on the concentration of i in the specimen, but also on the specimen matrix (S, γ_i^+) and the electronic properties of the surface (γ_i^+).

Many attempts have been made to develop a routine approach for quantitative SIMS analysis, but none has been successful. Currently, SIMS—at least in a practical sense—is limited to the quantitative analysis of the impurities, dopants, or minor elements detected in a depth profile or bulk impurity analysis; SIMS is not used extensively for quantitative analysis of the surface or bulk stoichiometry of unknowns. Because SIMS supersedes other techniques primarily in the analysis of dopants and trace impurities, this apparent limitation should not be viewed as a disadvantage.

A quantitative SIMS analysis requires independent knowledge of the sputtering rate (see the previous section in this article) and a calibration of the secondary ion signal using standards whose matrix and surface electronic properties match those of the specimen. The use of reactive primary ion beams facilitates reproduction of the surface electronic properties between the specimens and the standards. The methods for preparation and calibration of standards with matrices identical to the specimens are varied, but the ion implantation of known doses of the element of interest into the matrix of interest is unquestionably the most convenient (Ref 12). This approach is described below.

The use of ion-implanted standards for quantitative SIMS analysis assumes a linear relationship between the SIMS signal and the elemental concentration. That is, the product of I_p, S, γ_i^+, and η (see Eq 3) is assumed to be a constant for the specimen and the standard (at least during analysis). This is true only at low concentrations (that is, dopants and impurities in the sub-ppm to 1000-ppm range); at higher concentrations, the electronic and chemical properties of the matrix can become a function of this concentration. The basic concept behind the use of ion-implant standards is that the implant fluence F determines the total number of atoms implanted per unit area; F (atoms or ions per square centimeter) can be measured and controlled to within approximately 5%. Thus, the secondary ion signal, when integrated over the entire profile measured for the implant standard (Fig. 11a), can be related to the total number of implanted atoms contained in the specimen:

$$\int_0^z I_i^+(z)dz = K \int_0^z C_i(z)(dz) \qquad \text{(Eq 4)}$$

where z is the depth of the analysis, and K is a constant that accounts for the terms in Eq 3; that is, K is the calibration factor used to convert the secondary ion signal (I_i^+ in counts per second) measured over the range dz into an average concentration (C_i in atoms per cubic centimeter). If z exceeds or equals the maximum extent of implantation in the standard, all the implanted atoms per unit area will have been analyzed, and:

$$\int_0^z C_i(z)(dz) = F \text{ (atoms or ions/cm}^2\text{)} \qquad \text{(Eq 5)}$$

Thus, the calibration factor can be obtained by integrating the secondary ion signal over the depth z:

$$K = \frac{\int_0^z I_i^+(z)dz}{F} \qquad \text{(Eq 6)}$$

Because the secondary ion signal is measured over a time interval dt, it is apparent that an independent measure of the sputtering rate, $\dot{z}$, is required; then:

$$K = \frac{\dot{z}}{F} \int_0^t I_i^+(t)dt \qquad \text{(Eq 7)}$$

where t is the total time over which the profile is integrated.

The calibration constant K can now be used to convert the measured secondary ion signal into absolute concentration in atoms per cubic centimeter:

$$C_i = \frac{1}{K} I_i^+ \qquad \text{(Eq 8)}$$

The secondary ion signal is usually measured in counts per second (averaged over a time interval dt); therefore, the units of K are essentially (atoms/cm^3)/cps. This constant is valid only for element i in a matrix that is identical to that of the standard. Moreover, the concentration C_i in the unknown must be in the dilute range, and the instrumental parameters used during analysis of the unknown must be the same as those used to obtain K from the unknown. Ideally, the standard is analyzed along with the unknowns. However, when the specimens and instruments are well characterized and controlled, or it is impractical to examine the implanted standard repeatedly, a normalized calibration constant, K_n, can be determined.

It is assumed that the ratio of the terms in Eq 3 for the element i (I_i^+) and some matrix species $M(I_M^+)$ is constant, that is:

$$K_n = \frac{z}{F}\int_0^t \frac{I_i^+(t)}{I_M^+(t)}\,dt \qquad \text{(Eq 9)}$$

and then:

$$C_i = \frac{1}{K_n}\cdot\frac{I_i^+(z)}{I_M^+(z)} \qquad \text{(Eq10)}$$

Perhaps the most obvious use of the calibration factor K is for quantitative analysis of the ion-implantation profile itself (Fig. 11a). The quantitative analysis of ion-implantation profiles is an important application of SIMS in the microelectronics industry. In this case, the implanted specimens (assuming the implanted fluence is known) are self-standardizing; that is, the integrated profile provides the calibration factor that can be used to convert the instantaneous secondary ion signals to concentration units. This conversion is shown in Fig. 11(b) for the raw data plotted in Fig. 11(a). More common, though, is the use of K or K_n (obtained using the implanted standard) to convert the secondary ion signals from another sample.

Fig. 13 The relationship between the $^{120}Sn^+$ secondary ion signal (normalized to the $^{16}O^+$ signal) and the relative tin content of various tin-oxide-doped silicate glasses

This calibration curve has been used for quantitative analysis of tin-oxide profiles in gloss surfaces obtained in a scanning ion microprobe.

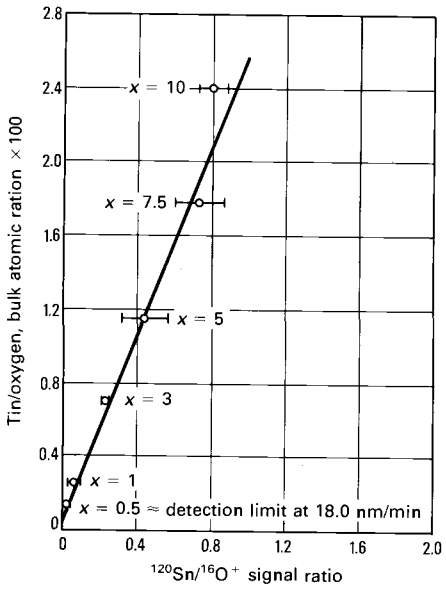

It is often desirable to use SIMS for quantitative analysis when concentrations from 0.1 to 10 at.% are of interest. In this case, it is necessary to verify the existence of a linear relationship between the secondary ion signal and the concentration. Thus, it is common to prepare a set of standards that bracket the concentration range of interest. The calibration curves shown in Fig. 13 and 14 illustrate these relationships for a glass matrix (where the analysis of tin is of interest) and a steel matrix (where the analysis of nickel is of interest). Once again, normalization of the secondary ion signal to a matrix species facilitates the definition of a practical calibration constant.

Ion Imaging

The acquisition of secondary ion images can be accomplished in one of two ways, depending on the instrument design (Fig. 15). In the case of the ion microprobe (Fig. 4 and 15a), the incident primary ion beam is focused to a small spot, then rastered over the sample surface. The analysis is carried out point by point, and the image is constructed by synchronizing the cathode ray tube (CRT) and the detector with the primary ion beam. That is, a particular secondary ion (for example, $^{27}Al^+$, FeO^+, and so on) is selected at the mass spectrometer, and its intensity variation from point to point is displayed on the CRT. This approach is analogous to that used for x-ray imaging in the electron microprobe. The resolution is determined by the diameter of the primary ion beam, typically 2 to 5 μm. In contrast, the ion microscope is a direct-imaging system in which the secondary ions are simultaneously collected over the entire imaged area (Fig. 5 and 15b). A strong electrostatic field between the specimen and the immersion lens preserves the spatial distribution of the emitted secondary ions. This secondary ion beam is then mass analyzed (only a double-focusing magnetic mass spectrometer is applicable for direct imaging), and in essence, the spatial distribution of the secondary ions is transmitted through the mass spectrometer. The transmitted secondary ions (for example, $^{27}Al^+$, FeO^+, and so on) then strike a microchannel plate, where the image is formed. The direct-imaging ion microscope can be compared to the transmission electron microscope or emission microscope. The resolution is determined by the optics of the system, for which the size of the imaged area on the specimen, that is, the field aperture, and the contrast aperture are major factors; however, the resolution is typically of the order of 0.5 to 1 μm.

Fig. 14 The relationship between the Ni^+ secondary ion signal and the nickel content of NBS standard reference steels 661, 662, 663, 664, and 665

This calibration curve can be used for quantitative analysis of nickel in comparable low-alloy steels using an ion microprobe. Source: Ref 13

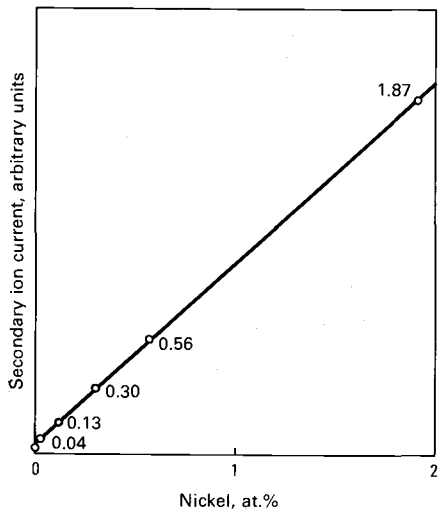

The interpretation of secondary ion images must be approached with caution. Because the secondary ion intensity depends not only on the concentration of the imaged species, but also on the chemical and electronic properties of the matrix, the image contrast from point to point may have many origins. In polycrystalline materials, for example, the differences in crystallographic orientation between grains can influence the adsorption of oxygen from the residual vacuum, the implantation of oxygen from the primary beam, or the sputtering rate. Any one of these can lead to contrast in the secondary ion image for one grain relative to the other, even though no concentration difference exists. This sensitivity to subtle differences in secondary ion yield between various microstructural features can be the major source of image contrast and is in fact the basis of the ion emission microscope. This microscope is used primarily for microstructural imaging and not necessarily for the microchemical analysis of interest in SIMS.

Nonmetallic Samples

The analysis of insulators (glasses, ceramics, geological materials, and polymers) presents "charging" problems in SIMS, and in general, special procedures and additional effort are required (Ref 14, 15). The charging problem associated with these materials is due to the high incident primary ion current relative to the much lower emitted secondary ion current; secondary electron

Fig. 15 Schematic diagrams of secondary ion imaging

(a) In a direct-imaging ion microscope. (b) In a scanning ion microprobe

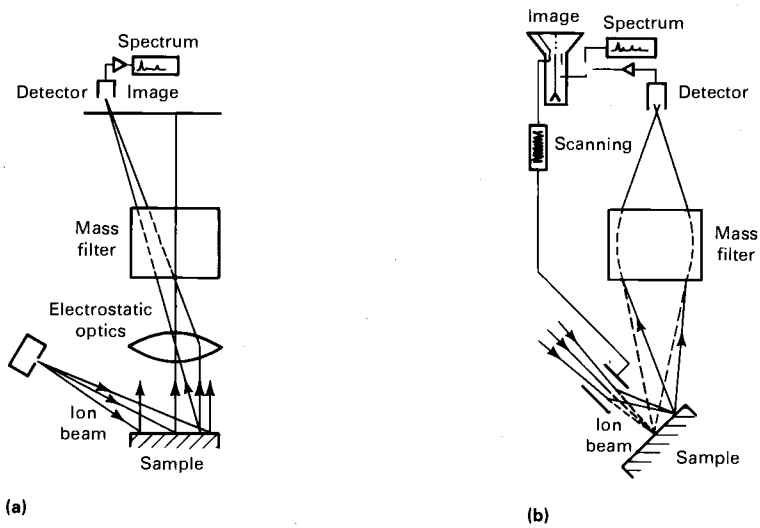

emission during ion bombardment further enhances the charge imbalance. All of this leads to a net positive charge at the surface (if positive primary ions are used), and the associated surface potential will influence the energy distribution of the emitted secondary ions. In general, the surface potential is unstable and thereby precludes the acquisition of meaningful spectra or depth profiles.

Several procedures have been established for the analysis of insulators, but the optimum method will depend on the specifics of the instrument and the materials. The most common approaches are (1) the deposition of metal coatings on the sample that are sputtered through to provide a path for local charge neutralization at the periphery of the ion beam crater, (2) use of metal grids or metal plates with apertures, which are placed over the sample for local charge neutralization, (3) auxiliary charge neutralization with an electron beam or flood gun, (4) use of a negative oxygen primary beam (O^-) that leads to a finite but stable surface potential after a few moments of bombardment, and (5) bombardment with a neutral beam (Ref 16). There is probably no substitute for experience in the analysis of insulators.

Another problem associated with the analysis of insulators, especially insulating thin films and coatings, is the migration of mobile ions due to the electric field generated by the ion-bombardment-induced surface potential. This migration can severely distort the in-depth profile of, for example, sodium, potassium, chlorine, fluorine, and so on, in oxide materials and films. The proper charge neutralization will greatly alleviate this effect, but its presence should always be considered.

Finally, the analysis of organic, biological, and other materials with volatile constituents also requires special approaches. It is common to freeze the specimen with liquid nitrogen using a cold stage. The mass spectra of organic and biological materials are exceedingly complex. The use of SIMS for the analysis of these materials must be carefully warranted, such as for trace metal detection in biological specimens, organic polymers, or films.

Detection Limits

It has been emphasized that one of the unique characteristics of SIMS is its high detection sensitivity relative to other surface microanalytical techniques. Nonetheless, it is important to recognize that the detection limit varies with the element, the sample matrix, and the operating procedures of the instrument (primary ion, sputter rate, instrument transmission, and background). For example, the detection limit in metallic, semiconducting, and other nonoxide matrices will be maximized only when reactive oxygen or cesium beams are used. When high spatial resolution, high depth resolution, or high mass resolution is also required, there will be some loss in detection sensitivity. There are at least two reasons for this.

One of these concerns the rate of material consumption, because this ultimately determines the total secondary ion count rate. If high spatial resolution is required in a microanalysis problem, for example, a reduction in the beam diameter will be necessary. This is often accompanied by a decrease in the beam current and therefore a decrease in the rate of material consumption, even though the sputtering rate $\dot{z}$ may increase. Similarly, a loss in sensitivity occurs when $\dot{z}$ is reduced at a constant spot size to enhance the resolution of in-depth profiles.

The other reason for a less than optimum detection sensitivity concerns the collection and transmission of the secondary ions. Any electronic or mechanical gating of the sputtered crater, such as that required for high-resolution in-depth profiling, will reduce the detected signal. Similarly, the need for high mass resolution will reduce the ion transmission in the mass spectrometer and again result in a loss in detection sensitivity. In addition, any background due to residual gas or primary ion beam contamination will further limit the detection sensitivity.

Because of the element and matrix dependence and the instrumental interdependences noted above, it is not possible to quote a unique detection sensitivity for SIMS. The detection limits will be maximized in a bulk impurity analysis in which the highest beam current can be used because neither depth nor spatial resolution are of concern; this assumes that low mass resolution can be tolerated. Under these conditions, the detection limits for most elements can be expected to be in the parts per billion to parts per million range, assuming an oxide matrix and/or a reactive-ion primary beam.

Applications*

Example 1: Surface Composition Effects During Laser Treatment of AISI Stainless Steel. Although lasers are used for processing many materials, laser welding is not an acceptable procedure for certain metal alloys. If an alloy contains one or more volatile components, selective vaporization of the more volatile components during laser welding may lead to inadequate control of the weld composition and poor mechanical properties of the fabricated product. The loss of alloying elements and the eventual properties of the weld zone are influenced by fluid flow in the weld pool, heat transfer, and the thermodynamics and kinetics of the vaporization of various components from the molten pool.

In this study, SIMS was used to examine the surface region of an AISI 202 stainless steel before and after various treatments with a CO_2 laser. Of particular interest were the effects on hydrogen and oxygen, because

*Example 5 was provided by G.C. Nelson, Sandia National Laboratories. This work supported by the U.S. Department of Energy under Contract No. DE-AC04-76DP00789.

Fig. 16 Negative SIMS depth profiles of oxygen and hydrogen as a function of the laser irradiation of an AISI 202 steel

Obtained using $^{133}Cs^+$ primary ion bombardment in an ion microscope

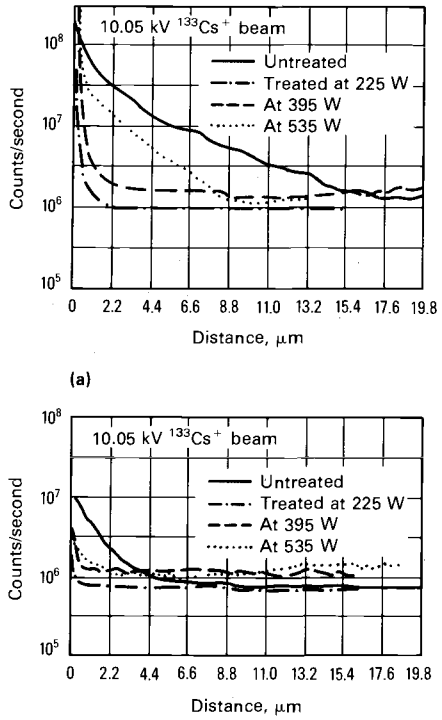

Fig. 17 High-resolution SIMS spectra for a phosphorus-doped silicon substrate

Obtained using $^{32}O_2^+$ primary ion bombardment in an ion microscope

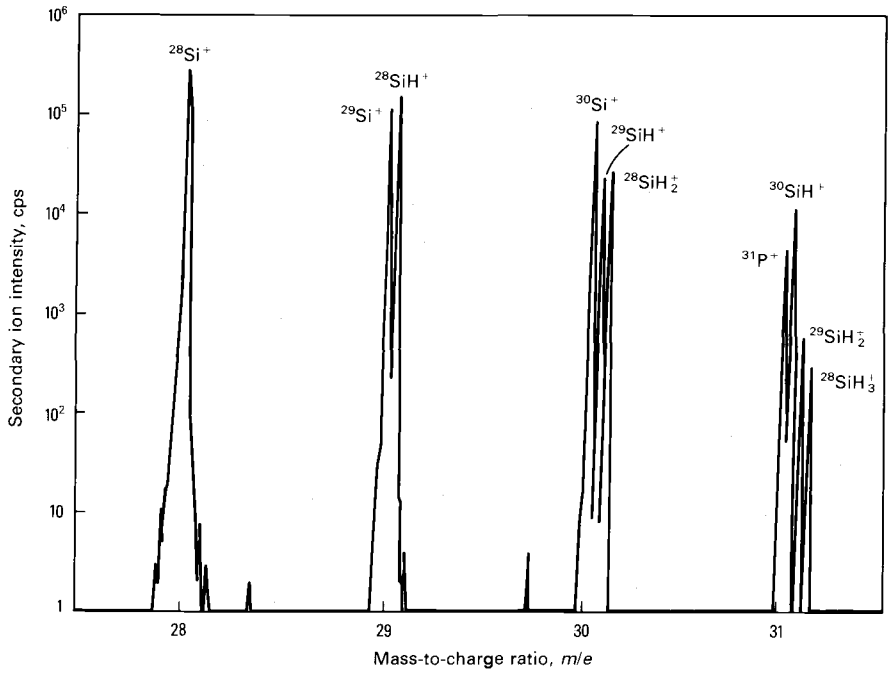

these species can profoundly influence mechanical and chemical properties. Figure 16 shows the oxygen and hydrogen depth profiles for selected samples analyzed using an ion microscope. A $^{133}Cs^+$ primary ion beam was used to enhance sensitivity to the $^{16}O^-$ and $^1H^-$ secondary ions.

It is apparent that the initial untreated surface is oxidized to a depth of the order of 10 μm; the surface also shows hydrogen penetration to approximately 5 μm. After the laser surface treatment, the oxygen and hydrogen contents of the irradiated surfaces have been reduced. A more careful inspection reveals, however, that the extent of this selective vaporization of oxygen and hydrogen is reduced with increasing power levels. These observations are being correlated with independent calculations and measurements of the depth of penetration of the laser treatment, the liquid pool temperature, and the corresponding change in concentration profile for the nickel, chromium, and manganese alloying agents. Although not shown, the latter are also measured with SIMS, but in that case, a $^{32}O_2^+$ primary ion beam is used to enhance the sensitivity and to attenuate the matrix effects for analysis of the Ni^+, Cr^+, and Mn^+ secondary ions. It has been found that the observed changes in concentration of the alloying elements are due to differences in their solubility in the ferrite and other nonequilibrium phases, which form after laser irradiation of the original austenitic steel. A quantitative analysis has not yet been attempted in this work, but could be conveniently accomplished by ion implantation of hydrogen, oxygen, nickel, chromium, manganese, and so on, in a specimen of AISI 202.

Example 2: Quantitative Analysis of a Phosphorus Ion-Implantation Profile in Silicon. Ion implantation is an important process for low-level, shallow doping of silicon microelectronic devices. Secondary ion mass spectroscopy is uniquely qualified to verify these implantation profiles for process development, quality control, and failure analysis. In this example, the use of SIMS is demonstrated for the analysis of phosphorus (an *n*-type dopant) after ion implantation into silicon. Due to the presence of hydrogen in the silicon matrix and in the residual vacuum, however, a spectral interference occurs at $m/e \approx 31$ between P^+ ($m/e = 30.9738$), $^{30}SiH^+$ ($m/e = 30.9816$), $^{29}SiH_2^+$ ($m/e = 30.9921$), and $^{28}SiH_3^+$ ($m/e = 31.0004$). Thus, a high-resolution mass spectrometer is necessary to separate the desired analyte species (P^+) from the molecular matrix ion interference (SiH^+, SiH_2^+, and SiH_3^+).

Figure 17 shows a high-resolution SIMS spectrum for the region $m/e = 28$ to 31, where the separation of the isotopic silicon and silicon-hydride species is demonstrated. It would not be possible to verify unequivocally the presence or concentration of phosphorus in this semiconductor without the high-resolution capability. This level of resolution cannot be attained using a quadrupole, where resolution is typically 1 atomic mass unit (amu). The mass resolution of this double-focusing magnetic sector is 10 to 100 times better; therefore, species whose mass-to-charge ratios differ by fractions of 1 amu can be separated.

Because the instrument has in this case been optimized for mass resolution, a loss in the detection sensitivity for phosphorus must be tolerated. However, the profile in Fig. 18(a) reveals that the sensitivity using a reactive $^{32}O_2^+$ primary ion beam is sufficient to measure the implantation profile over a dynamic range of 10^4 cps. It can also be seen that although the $^{31}P^+$ signal varied over four orders of magnitude through the profile, the $^{28}S^{2+}$ matrix signal ($m/e = 13.9885$) was constant (due to the use of an oxygen primary ion beam). After the profiling anal-

Fig. 18 Phosphorus depth profiles for an ion-implanted silicon substrate

(a) Before quantitative analysis of the positive SIMS data. (b) After quantitative analysis. Obtained using $^{32}O_2^+$ bombardment in an ion microscope. Obtained using $^{133}Cs^+$ beam bombardment in an ion microscope

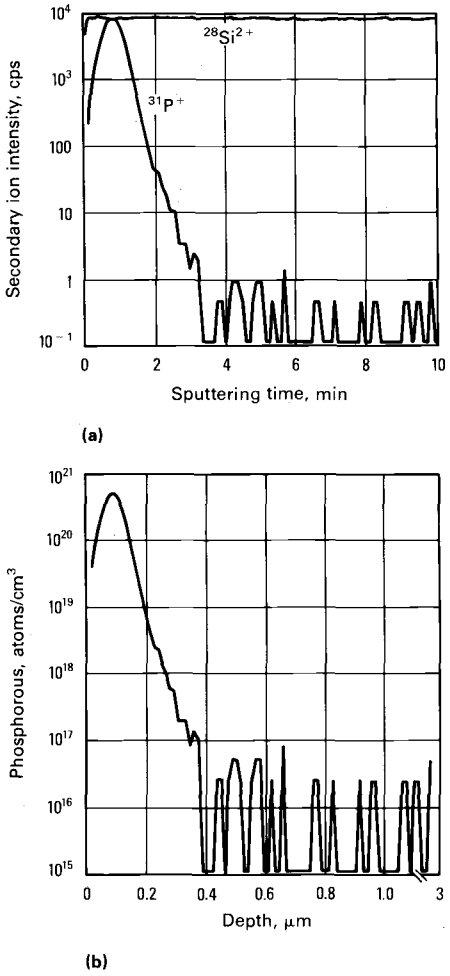

ysis was complete (approximately 10 min of sputtering), the depth of the sputtered crater was measured independently using a profilometer; the depth was found to be approximately 0.11 μm to yield a sputtering rate of 110 nm/min. The fluence used to prepare this implant was known; therefore, a quantitative analysis could be performed without an external standard. That is, the quantified profile shown in Fig. 18(b) was obtained using Eq 7 and 8. The background concentration represents less than 1 ppm P.

Example 3: Quantitative Impurity Analysis in LPCVD Thin Films. Low-pressure chemical vapor deposition (LPCVD) is used extensively for the preparation of thin films. In this example, the relationship between the reactive and residual gases in the chemical vapor deposition (CVD) reactor is of interest, as are the composition and hydrogen impurity content of silicon-oxynitride films. Figures 19(a) and (b) present two quantified profiles for SiO_xN_y films deposited on silicon with different process parameters. In both cases, the films were deposited at 910 °C (1670 °F) with a total gas pressure of 0.4 torr, and the silicon source was $Si_2H_2Cl_2$ gas. The film shown in Fig. 19(a) used an ammonia (NH_3) to nitrous oxide (N_2O) ratio of 3; the film shown in Fig. 19(b) was deposited with an NH_3/N_2O ratio of 1/3. The average silicon/nitrogen ratio of the films was not significantly affected by the NH_3/N_2O ratio, but the relative concentrations of oxygen and hydrogen were influenced. The analysis of many SiO_xN_y films processed under different conditions has revealed that NH_3 is a more efficient source of nitrogen than is N_2O and that the NH_3 activity determines the hydrogen level in the film.

The quantitative analyses represented in Fig. 19(a) and (b) were performed using selected silicon-oxynitride thin films whose absolute hydrogen, nitrogen, and oxygen concentrations were independently calibrated using RBS and nuclear reaction analyses. These standards were then used to calibrate the secondary ion signals for the other specimens. The sputtering rate was determined by independently measuring the film thickness with ellipsometry, then observing the time necessary to sputter through the film to the SiO_xN_y/Si interface.

Example 4: Glass Surface Layer Analyses. The use of SIMS for depth-profiling three (unrelated) glass specimens after surface treatment or corrosion is described in this example. Figure 20 shows the

Fig. 19 Negative SIMS depth profiles for LPCVD SiO_xN_y thin films on silicon

(a) NH_3/N_2O = 3 during deposition. (b) NH_3/N_2O = 0.33 during deposition. Obtained using $^{133}Cs^+$ beam bombardment in an ion microscope

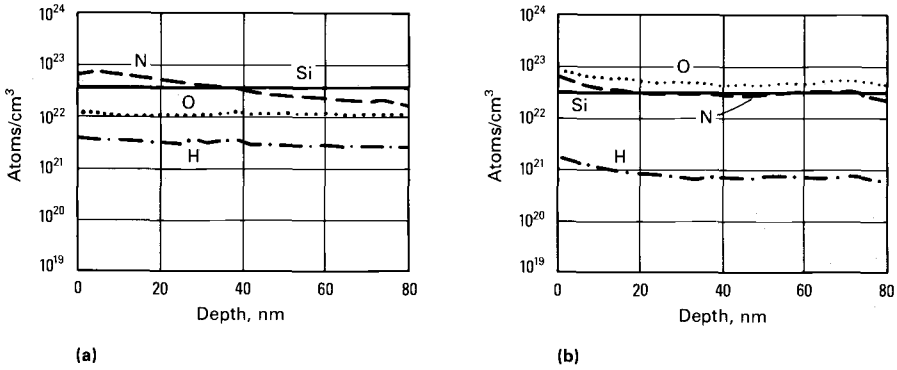

Fig. 20 Positive SIMS depth profiles

(a) Various constituents. (b) Hydrogen in a calcium-boroaluminosilicate glass ribbon after acid-etching 16 h in H_2SO_4. Obtained using Ar^+ primary ion bombardment in a scanning ion microprobe and an electron beam for charge neutralization

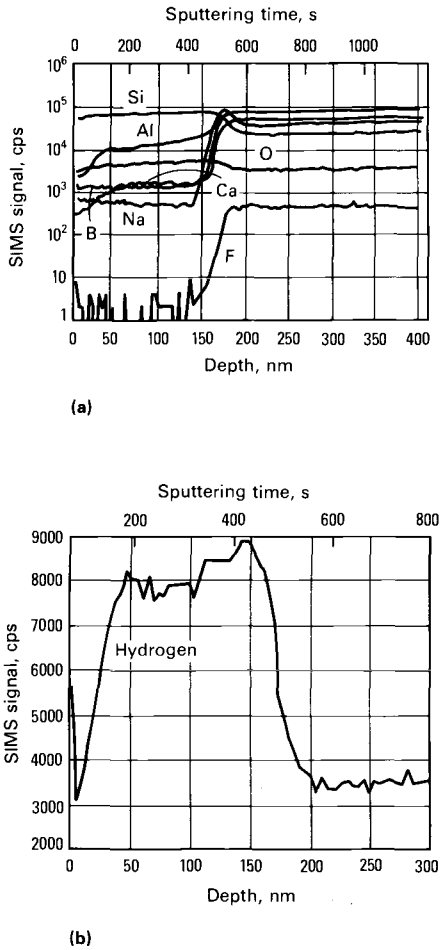

profiles for a multicomponent calcium-boroaluminosilicate glass ribbon after an acid-etching treatment. The presence of a surface film approximately 200 nm in thickness is evident after 16 h in concentrated sulfuric acid. The surface layer forms due to preferential leaching of the acid-soluble aluminum, boron, calcium, and sodium oxides and fluorides. The insoluble silica remains intact on the glass surface as a hydrated surface layer; the corresponding hydrogen profile is shown in Fig. 20(b). In this application, the kinetics and chemical mechanisms of this leaching process could be followed without the need for a quantitative compositional analysis. These profiles were obtained in an ion microprobe using an inert argon ion beam and raster gating; the charge neutralization was accomplished using an electron beam.

Figure 21(a) shows the profiles for an alkali-lead-silicate glass (commonly termed crystal) that exhibited a haze due to weathering in a humid atmosphere. The haze is essentially a surface film that can be easily removed by rinsing in cold water. Thus, the profiles shown in Fig. 21(b) represent a piece of the same glass specimen shown in Fig. 21(a) after rinsing in deionized water. The secondary ion signals for the various elements in this alkali-lead-silicate glass were normalized to the $^{29}Si^{4+}$ signal to facilitate comparison of the profiles for the hazed and cleaned surfaces.

It is evident that the haze is rich in sodium and potassium (probably hydroxides), which were leached to the surface from depths of the order of 200 to 300 nm; that is, regions depleted of sodium and potassium are apparent in the subsurface. The corresponding penetration of hydrogen to depths of the order of 200 to 300 nm indicates that water in the ambient atmosphere is probably responsible for this corrosion reaction. This glass surface, even after the cleaning, is permanently hydrated and depleted of sodium and potassium. Thus, subsequent exposure to a moist atmosphere requires a greater length of time to regenerate visible haze.

These profiles were obtained in an ion microscope using a $^{18}O^-$ primary ion beam; the negative primary ions were used to eliminate unstable charging of the surface. Although an electron beam could also have been used for charge neutralization, this often leads to electron-stimulated desorption and decomposition of weakly absorbed surface species, such as alkali hydroxides. The $^{18}O^-$ isotope was used to permit analysis of the $^{16}O^+$ that is intrinsic to the specimen.

Figures 22(a) and (b) compare the in-depth profiles of an alkali-lead-silicate glass before and after a hydrogen reduction treatment. This treatment produces a thin black semiconducting layer at the glass surface that is critical to the fabrication of microchannel plates and other charged particle detectors. The kinetics of the hydrogen diffusion and reduction reaction are easily followed using the $^1H^+$ secondary ion profile. It is also noteworthy that sodium has been depleted to some extent during the hydrogen reduction (probably due to vaporization); this alkali depletion can influence the work function and secondary electron yield of the devices.

Example 5: Determining Isotopes of Oxygen in an Explosive Actuator. Secondary ion mass spectroscopy is unique among surface analytical techniques for its

Fig. 21 Positive SIMS depth profiles for alkali-lead-silicate crystal glass

(a) Hazed surface. (b) Cleaned surface. Obtained using $^{18}O^-$ primary beam bombardment in an ion microscope

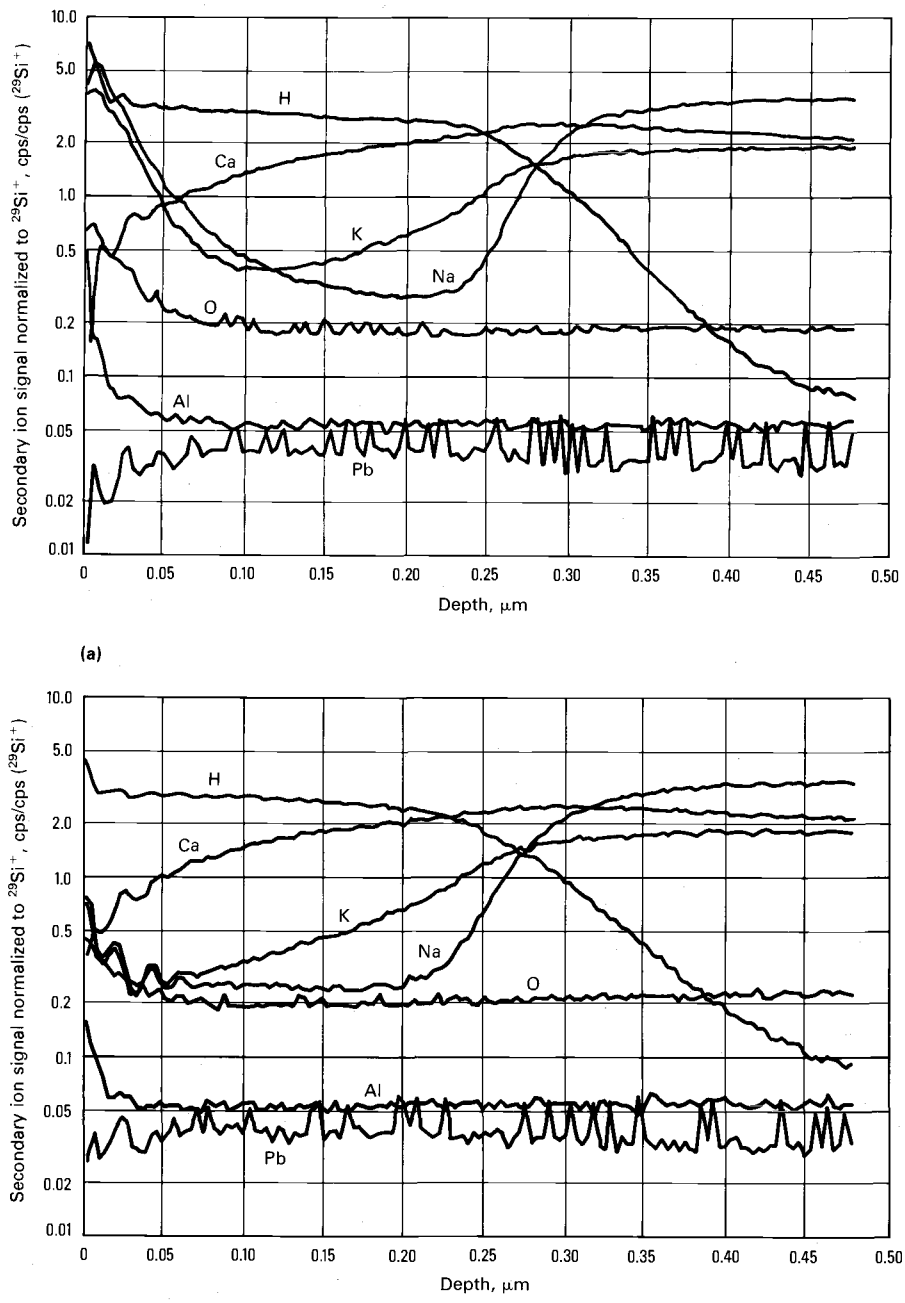

Fig. 22 Positive SIMS depth profiles for a lead-silicate glass

(a) Before and (b) after hydrogen reduction to produce a semiconducting surface layer. Obtained using $^{32}O_2^+$ primary beam bombardment and electron beam charge neutralization in an ion microscope

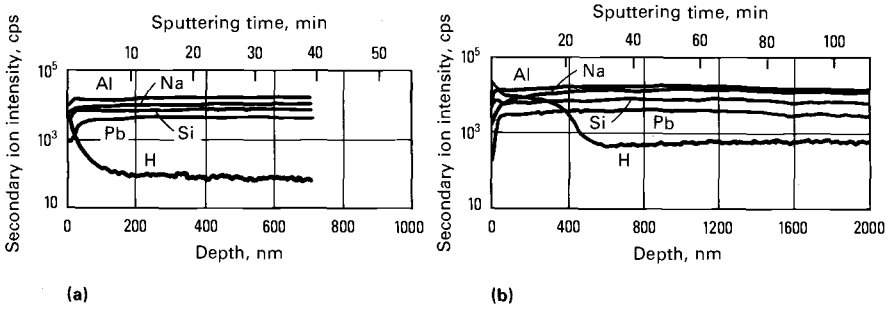

ability to detect hydrogen and to distinguish among the various isotopes of an element. This latter capability is very useful when studying the oxidation process in that ^{18}O can be used to differentiate between the oxidation that occurs during the experiment and any oxide (from ^{16}O) that may have been present before the experiment. An example of the use of SIMS to help determine the cause of enhanced output of an explosive actuator will be discussed.

The explosive actuator of interest consists of TiH_x powder mixed with $KClO_4$ powder. The powders are ignited by an electrically heated bridgewire. After extended periods of storage, these actuators experienced outputs of explosive energy that were considerably greater than their nominal value. One of the possible explanations for this occurrence was that the natural TiO_2 layer that exists on the surface of the TiH_x powder was reduced during shelf life, allowing a faster reaction with the $KClO_4$. Due to the high free energy for the oxidation of titanium, it was thought to be impossible to open the actuators and transport them to a surface analysis apparatus to locate reduced titanium. Instead, it was decided to open the actuators in an ^{18}O environment so that the elemental titanium, if present, would react with the ^{18}O, forming $Ti^{18}O_2$. Secondary ion mass spectroscopy would then be used to locate the $Ti^{18}O_2$.

Fig. 23 Spectra obtained from a $TiH_x/KClO_4$ sample exposed to ^{18}O

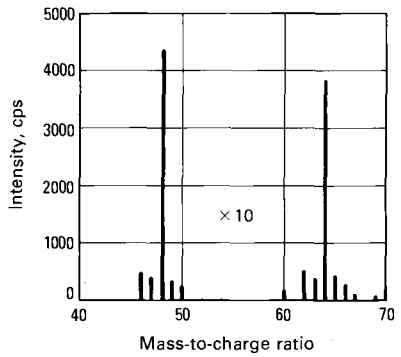

Five sample materials were analyzed. Two of the samples, TiH_x and $TiH_x/KClO_4$, were used to obtain baseline data in terms of which molecular ion species were present. The other three samples, all of which were $TiH_x/KClO_4$, were exposed to ^{18}O. The positive SIMS spectra in the mass-to-charge region of 45 to 70 amu were recorded for each of the above samples. This region contains the lines of the elemental titanium isotopes and the various molecular ions associated with titanium, ^{16}O, ^{18}O, and hydrogen.

Figure 23 shows an example of the spectra obtained from an ^{18}O-exposed sample. The peaks due to the various molecular ions are indicated. Because there is considerable peak overlap among the possible molecular ion species, a linear least squares analysis was used to separate the ^{18}O contribution. In this method, standard spectra for each elemental and molecular ion are linearly combined to obtain the best least squares fit to the experimental data. The result of the fit provides the contribution of each component to the experimental spectra. To determine the absolute concentration of each component, a sensitivity factor for each component must be known. These were not known for the current case, and absolute quantification was not attempted. However, because molecular ions due to $Ti^{16}O$ were easily observed, it was assumed that ions due to $Ti^{18}O$, if present, would be observed with the same sensitivity.

The standard spectra for each molecular species used in the least squares fitting were calculated from tables of isotopic abundances. Standard spectra were calculated for titanium, $Ti^{16}O$, $Ti^{18}O$, TiH, TiH_2, $Ti^{16}OH$, $Ti^{18}OH$, $Ti^{16}OH_2$, and $Ti^{18}OH_2$. Table 2 shows the results from one of the samples. In all three cases analyzed, the ^{18}O contribution was zero within experimental error. These results indicate that for the samples used in these experiments the surface $Ti^{16}O_2$ layer had not been reduced and thus was not the source of the enhanced output of the explosive actuator.

Table 2 Results of SIMS analysis of an explosive actuator

Component	Intensity, *I*
Ti	5659
TiH	79.5
TiH_2	−3
$Ti^{16}O$	512
$Ti^{16}OH$	14
$Ti^{16}OH_2 + Ti^{18}O$	−0.6 ± 0.6
$Ti^{18}OH$	1.1 ± 1.8
$Ti^{18}OH_2$	−0.2 ± 0.3

REFERENCES

1. G. Garter and J.S. Colligon, *Ion Bombardment of Solids*, Heinemann, 1968
2. M. Kamisky, *Atomic and Ionic Impact Phenomena on Metal Surfaces*, Springer-Verlag, 1965
3. O. Auciello and R. Kelly, Ed., *Ion Bombardment Modification of Surfaces*, Elsevier, 1984
4. G.K. Wehner, in *Methods of Surface Analysis*, A.W. Czanderna, Ed., Elsevier, 1975, p 5-38
5. A. Benninghoven, *Crit. Rev. Solid State Sci.*, Vol 6, 1976, p 291
6. K. Wittmack, in *Ion Beam Surface Layer Analysis*, Vol 2, O. Meyer *et al.*, Ed., Plenum Press, 1976, p 649-658
7. C.W. Magee, W.L. Harrington, and R.E. Honig, *Rev. Sci. Instrum.*, Vol 49, 1978, p 477
8. J.M. Ruberol, M. Lepareur, B. Autier, and J.M. Gourgout, in *8th International Conference on X-Ray Optics and Microanalysis*, D.R. Beaman, Ed., Pendell Publishing, 1979, p 322-328
9. C.W. Magee and E.M. Botnick, *J. Vac. Sci. Technol.*, Vol 19 (No. 1), 1981, p 47
10. W.L. Fite and M.W. Siegel, "Energy Filters for Secondary Ion Mass Spectrometry," Extranuclear Laboratories, Pittsburgh, 1977
11. R.J. Blattner and C.A. Evans, Jr., *Scan. Elec. Microsc.*, Vol IV, 1980, p 55
12. D.P. Leta and G.H. Morrison, *Anal. Chem.*, Vol 52 (No. 3), 1980, p 514
13. D.E. Newbury *et al.*, in *Surface Analysis Techniques for Metallurgical Applications*, STP 596, ASTM, Philadelphia, 1976, p 101-113
14. H.W. Werner and A.E. Morgan, *J. Appl. Phys.*, Vol 47, 1976, p 1232

15. K. Wittmack, *J. Appl. Phys.*, Vol 50, 1979, p 493
16. D.J. Surman and J.C. Vickerman, *Appl. Surf. Sci.*, Vol 9, 1981, p 108

SELECTED REFERENCES

- A. Benninghoven *et al.*, Ed., *Secondary Ion Mass Spectrometry—SIMS II*, Springer-Verlag, 1979
- G. Blaise, in *Materials Characterization Using Ion Beams*, J.P. Thomas and A. Cachard, Ed., Plenum Press, 1978, p 143-238
- J.W. Colbrun and E. Kay, in *CRC Crit. Rev. Solid State Sci.*, Vol 4 (No. 4), 1974, p 561
- R.J. Colton, *J. Vac. Sci. Technol.*, Vol 18 (No. 3), 1981, p 737
- K.F.J. Heinrich and D.E. Newbury, Ed., *Secondary Ion Mass Spectrometry*, NBS 427, National Bureau of Standards, Gaithersburg, MD, Oct 1975
- H. Liebl, *Anal. Chem.*, Vol 46 (No. 1), 1974, p 22A
- J.A.McHugh, in *Methods of Surface Analysis*, A.W. Czanderna, Ed., Elsevier, 1975, p 223-278
- G.H. Morrison and G. Slodzian, *Anal. Chem.*, Vol 47 (No. 11), 1975, p 932A
- N. Shimizu and S.R. Hart, in *Annual Review of Earth and Planetary Sciences*, Vol 10, Annual Reviews, 1981
- N. Winograd, in *Progress in Solid State Chemistry*, Vol 13, Pergamon Press, 1982, p 285-375
- E. Zinner, *Scanning*, Vol 3, 1980, p 57